Plasmonics of 3-D Nanoshell Dimers Using Multipole Expansion and Finite Element Method

Christopher G. Khoury,[†,‡] Stephen J. Norton,[†,‡] and Tuan Vo-Dinh[†,‡,§,*]

[†]Fitzpatrick Institute of Photonics, [‡]Department of BME, and [§]Department of Chemistry, Duke University, Durham, North Carolina 27708

ABSTRACT The spatial and spectral responses of the plasmonic fields induced in the gap of 3-D nanoshell dimers of gold and silver are comprehensively investigated and compared *via* theory and simulation using the multipole expansion (ME) and the finite element method (FEM) in COMSOL, respectively. The E-field in the dimer gap was evaluated and compared as a function of shell thickness, interparticle distance, and size. The E-field increased with decreasing shell thickness, decreasing interparticle distance, and increasing size, with the error between the two methods ranging from 1 to 10%, depending on the specific combination of these three variables. This error increases several fold with increasing dimer size, as the quasi-static approximation breaks down. A consistent overestimation of the plasmon's fwhm and red shifting of the plasmon peak occurs with FEM, relative to ME, and it increases with decreasing shell thickness and interparticle distance. The size effect that arises from surface scattering of electrons is addressed and shown to be especially prominent for thin shells, for which significant damping, broadening, and shifting of the plasmon band is observed; the size effect also affects large nanoshell dimers, depending on their relative shell thickness, but to a lesser extent. This study demonstrates that COMSOL is a promising simulation environment to quantitatively investigate nanoscale electromagnetics for the modeling and designing of surface-enhanced Raman scattering (SERS) substrates.

*Address correspondence to
tuan.vodinh@duke.edu.

The field of plasmonics, more specifically, nanoparticle surface plasmons, has experienced a recent surge in interest following the discovery that surface plasmons are responsible for enhancements of the local E-field in the vicinity of metallic, nanostructured surfaces. Such enormous enhancements, up to 10^{14},[1] have enabled Raman scattering, an intrinsically weak scattering phenomenon, to become an important detection methodology that provides narrow spectral resolution, wealth of molecular information, and potential sensitivity for single molecular detection;[2,3] this is known as the field of surface-enhanced Raman scattering (SERS).

Plasmon resonances arise within a metallic nanoparticle from the collective oscillation of free electrons driven by an incident optical field. The plasmonic response of nanoparticles has played a role in a growing number of applications, including SERS, chemical sensing, drug delivery, photothermal cancer therapy, and new photonic devices. Our laboratory has been involved in the investigation and application of plasmonic nanosubstrates for SERS detection for over two decades. Since our first report on the practical analytical use of the SERS techniques for the trace analysis of a variety of chemicals, including several homocyclic and heterocyclic polyaromatic compounds in 1984,[4] our laboratory has been involved in the development of SERS technologies for applications in chemical sensing, biological analysis, and medical diagnostics.[5−11]

The wealth of experimental protocols and data in the literature for synthesizing SERS substrates, both *via* wet chemistry[10,12−15] or on fixed substrates,[16−18] necessitates numerical methods that confidently solve nanoscale electromagnetics of 3-D geometries with high spatial and spectral resolution; this is essential for understanding the fundamentals of the already available SERS substrates, as well as for further exploring and optimizing future substrate designs.

The Mie theory provides the exact analytical description of the behavior of the E-field surrounding isolated spherical nanoparticles but is unfortunately strictly limited to the spherical geometry. It cannot be employed to solve more interesting and realistic problem, consisting of irregularly shaped structures that are arbitrarily positioned in space. The analysis of such geometries requires numerical methods to solve Maxwell's equation in the computational domain *via* iterative procedures. The literature details two important computational electrodynamics modeling techniques to this end: the finite difference time domain (FDTD) and the finite element method

(FEM). Due to the nature of its discretizing algorithm, however, FDTD possesses intrinsic limitations for solving the electromagnetics problem at boundaries.[19−21] A recent report[20] evaluating FDTD as a method for solving the electromagnetic fields around metallic dimer nanoparticles demonstrated only a fair ability to do so, conveying large inconsistencies in field amplitude and plasmon peak position. This would suggest FEM as a more suitable approach when near-field optics are of interest.

COMSOL Multiphysics is a numerical simulation package based on FEM that allows accurate resolving of nanoscale electromagnetics in the vicinity of irregular nanostructures. Its accuracy relative to analytical theory is therefore of utmost importance for accurate characterization and design of such geometries. COMSOL has recently been used by several groups for modeling the plasmonics of nanoshells,[22−24] as well as other nanoscale geometries,[25−27] but these groups have focused exclusively on 2-D geometries. Ehrhold et al.[28] only briefly discussed the use of COMSOL for modeling the plasmonic properties of 3-D bimetallic nanoshells. The lack of 3-D modeling in COMSOL is a result of the significant time and computational power required to solve even a trivial problem in 3-D space. Nevertheless, there is significant discrepancy between 2-D and 3-D solutions, so much so that 2-D models are unable to reconcile experimental observation and numerical analysis.

This report comprehensively investigates the behavior of the fields around gold and silver nanoshell dimers in 3-D space, solved using ME implemented in MatLab and FEM within COMSOL. Clusters of nanoparticles under optical illumination have become the subject of recent analytical studies because of the potentially large field enhancements between the particles arising from surface plasmon resonances. Spherical dimers composed of pairs of solid nanospheres as well as linear chains of nanospheres have been analytically derived by several researchers.[29,30] The nanoshell dimer, however, represents a more versatile geometry that exhibits stronger field enhancements in its gap, relative to an isolated nanoshell, while boasting plasmon tuning capabilities by variations in shell thickness; both properties are important criteria of a good SERS substrate. Nanoshell dimers have recently been investigated both theoretically, using the plasmon hybridization method,[31] and numerically, by employing the FDTD method.[21] The plasmon hybridization method expresses the nanoshell dimer plasmon as a linear combination of the primitive plasmons, associated with the individual nanoshells, that electromagnetically interact and effectively "hybridize". The second report used the FDTD method to analyze the optical properties of silver nanoshell dimers and unraveled the FDTD as being prone to inherent numerical staircasing errors when attempting to map a curved surface on a Cartesian grid.

Because the synthesis and intricate control of the nanoshell dimer configuration has already been achieved,[32] it is of interest to identify other promising analytical and numerical methods that are able to accurately model this geometry. This paper extends Norton et al.'s ME analysis of a solid dimer[30] to a nanoshell dimer and complements the two aforementioned reports by comparing the spatial and spectral responses of the E-field between ME and FEM as a function of dimer size, shell thickness, and interparticle separation. The paper concludes with a final section that discusses the effects brought about by the incorporation of the size effect factor in the dielectric function, which arises when the particle size becomes comparable to the electron scattering mean free path length. To the best of our knowledge, this report is the first study that comprehensively benchmarks COMSOL's numerical algorithm based on FEM to the ME analytical method for solving a 3-D nanoshell dimer geometry, providing relative errors between the two for a number of important plasmon resonance band variables as a function of geometry.

RESULTS AND DISCUSSION

The versatility of gold and silver nanoshells for use in plasmonics originates from the fact that their plasmon resonance peaks can be controllably tuned throughout the visible region by adjusting the ratio of core to shell radii.[33] The dimer configuration results in plasmon coupling between the two nanoparticles, effectively concentrating the local E-field relative to that induced by a single nanoparticle, or monomer. The tunability of dimers is expected to follow a similar trend as for monomers, with possible differences stemming from additional plasmonic coupling behavior due to the particles' close proximity.

From a simulation perspective, the nanoshell dimer provides several degrees of freedom to test COMSOL's ability to mesh and solve at nanoscale resolutions: shell thickness $s = 1 - r_1/r_2$ in %, interparticle separation d in nanometers, and particle diameter $D = 2r_2$ in nanometers. These are depicted in the schematic of the 3-D nanoshell dimer model employed throughout the study (Figure 1). For conciseness, unique geometry combinations that define the nanoshell dimer geometry are represented using the "ND [D,d,s]" format, such that ND [20 nm,5 nm,Δs] indicates the study of a nanoshell dimer of diameter $D = 20$ nm and interparticle separation $d = 5$ nm as a function of shell thickness s. Due to the polarization selectivity of the plasmon excitation, the incident source was polarized with the electric field parallel to the bisphere axis, which effectively excites the dominant "longitudinal" plasmon of the system. This is the optimal polarization for creating the largest field enhancement in the gap between the particles. As such, the incident source was represented by a normal-
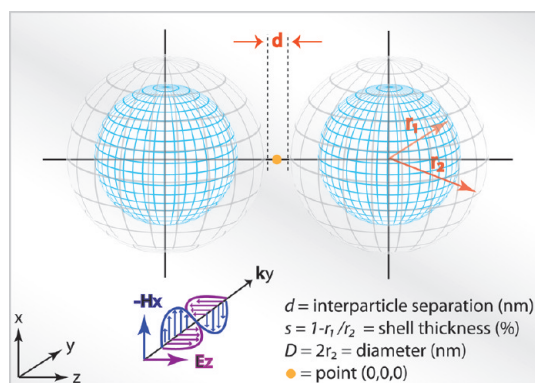
Figure 1. Schematic of the 3-D nanoshell dimer.

ized *z*-polarized TM wave, propagating in the *x*-direction.

Although the corresponding SERS enhancement would be approximately proportional to E_z^4,[34] the E-field magnitude $|E_z|$ is employed in this report for visualization purposes. Since the incident wavelength was set such that $|E_z|_{inc} = 1$, the computed $|E_z|$ is in fact representative of E-field enhancement: Enhancement = $|E_z|/|E_z|_{inc} = |E_z|$. In this report, we are particularly interested in computing the maximum E-field enhancement in the gap between the two nanoshells, at point (0,0,0). Throughout the remainder of the report, the variation of $|E_z|$ as a function of wavelength will be represented by the function $F_E(\lambda)$.

The gold and silver dielectric functions were modeled using the Lorentz−Drude dispersion model:[35]

$$\varepsilon(\omega) = 1 + \sum_{k=1}^{6} \frac{\Delta\varepsilon_k}{-a_k\omega^2 - ib_k\omega + c_k} \qquad (1)$$

where $\Delta\varepsilon_k$, a_k, b_k, and c_k are constants that provide the best fit for either metal.[35] The refractive index of the silica comprising the core of each particle was taken as 1.45 and assumed to be wavelength independent.[36,37] The surrounding medium was defined as air.

The ME employed in our study is based on the quasi-static approximation for which the particles are assumed to be much smaller than an optical wavelength, such that the incident electric field may be assumed to be uniform over the dimensions of the particle. The basic approach can be extended to the full-wave problem in which retardation affects are accounted for. The reduced complexity of the quasi-static approximation greatly simplifies the solution to the nanoshell dimer geometry, compared to that involving a full expansion of the Mie scattering coefficients, while boasting a similar accuracy for small nanoparticles. This size limitation has been claimed to be ∼λ/20,[38] beyond which the approximation progressively breaks down and the ME loses validity. In treating a dimer or cluster of spheres, the ME method is sometimes called the superposition method[39] since the scattered field can be expressed as

a superposition of the field scattered from each particle in the cluster. An advantage of this approach is that its accuracy can be easily evaluated by checking the convergence of the multipole expansion, undertaken by adding additional higher order terms until convergence is evident. The ME method can be very accurate and is often used as a benchmark against which other algorithms may be evaluated,[39] and its derivation is detailed in the Supporting Information.

COMSOL Multiphysics is a FEM-based numerical simulation package, which interfaces with MatLab and provides a number of modules for physics and engineering applications. The RF module was employed to characterize the electromagnetic fields in the computation domain comprising the nanoshell dimer. Maxwell's equations are simplified according to the selected application mode, which in this case is TM incidence, and are encompassed in a system of matrices. For 2-D geometries with a small number of degrees of freedom (DoF), a direct solver is able to solve the inverse problem, but for 3-D problems, an iterative solver iterates through the system until convergence is reached.

Accuracy of ME Relative to Mie Theory. The exact Mie theory solution for an isolated sphere is represented as an expansion of coefficients of the form $(a/\lambda)^{2n+1}$ with alternating sign, which converges very rapidly when $a \ll \lambda$ where a is the particle radius. Thus, the first term in the Mie expansion is proportional to $(a/\lambda)^3$ and the second term to $(a/\lambda)^5$. The magnitude of the first two terms are given by[40]

$$|a_1| = \frac{2}{3}\left|\frac{\varepsilon(\omega) - \varepsilon_0}{\varepsilon(\omega) + 2\varepsilon_0}\right|\left(\frac{2\pi a}{\lambda}\right)^3 \qquad (2)$$

$$|a_2| = \frac{1}{15}\left|\frac{\varepsilon(\omega) - \varepsilon_0}{2\varepsilon(\omega) + 3\varepsilon_0}\right|\left(\frac{2\pi a}{\lambda}\right)^5 \qquad (3)$$

The ratio of these terms is

$$\frac{|a_2|}{|a_1|} = \frac{1}{10}\left|\frac{\varepsilon(\omega) + 2\varepsilon_0}{2\varepsilon(\omega) + 3\varepsilon_0}\right|\left(\frac{2\pi a}{\lambda}\right)^2 \qquad (4)$$

The quasi-static approximation retains only a_1, such that the resonance plasmon peak is predicted to occur at a frequency determined by the condition Re$\{\varepsilon(\omega) + 2\varepsilon_0\} = 0$.

As an illustration, the value of the ratio 4 using the Lorentz−Drude dispersion model 1 is computed. Using the parameters for silver, the quasi-static approximation predicts a resonance peak at a wavelength of 370 nm. Evaluating eq 4 at this wavelength and for a particle radius of 10 nm results in a ratio of 0.001. For a solid sphere, the quasi-static approximation is equivalent to assuming a spatially uniform incident electric field (*i.e.*, the limit as λ → ∞), in which case the external field is equivalent to that of a dipole residing at the
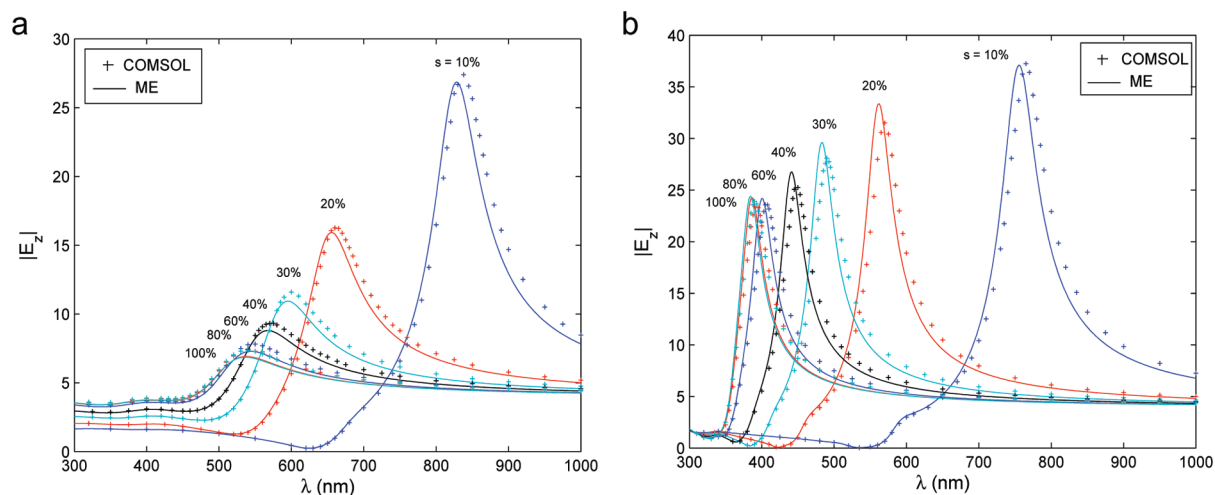
Figure 2. $F_E(\lambda)$ *vs shell thickness s for ND [20 nm,5 nm,Δs] of (a) Au and (b) Ag.*

sphere's center. The second term, given by eq 3, corresponds to a quadrupole response and is maximum when the real part of the denominator of eq 3 vanishes. This defines a quadrupole resonance, and at this wavelength, one might expect that the quasi-static approximation would fare poorly. However, using the above parameters for silver and evaluating eq 4 at the wavelength of the quadrupole resonance ($\lambda = 357$ nm), the ratio evaluates to 0.002, which is still very small. It is also worth noting that the second term in an infinite series with alternating sign, such as the Mie series, provides an upper bound to the error that results from dropping all terms in the series except the first. The above example for a solid sphere illustrates the dominance of the first term of the Mie series for small particles and may be regarded as providing further support for the validity of the quasi-static approximation under these conditions. Although the above results hold for an isolated spherical particle, similar arguments should hold for more complex objects, such as dimers.

The small divergence between the solutions of the ME and the Mie theory for 20 nm nanoparticles suggests that this diameter is small enough for the quasi-static approximation to hold; it is therefore employed as the nominal size for comparisons between ME and COMSOL.

Analysis of the E-Field as a Function of Wavelength. *Effect of Shell Thickness, Δs.* The plasmon resonance tunability was investigated for 20 nm nanoshell dimers of gold and silver, by varying the shell thickness s while keeping the interparticle distance fixed at 5 nm (or 25% of the particle diameter) and evaluating $|E_z|$ at the origin (0,0,0) for the wavelength range of 300−1000 nm. This separation was chosen to test COMSOL's ability to spatially resolve a narrow gap in a medium with a real, positive dielectric constant (free space), while varying the adjacent subdomains (shells) that are modeled by a complex dielectric function with a negative real part. The computed $F_E(\lambda)$ curves are plotted in Figure 2.

The figures clearly depict a red shifting of the resonance bands, as well as an increase in $|E_z|$ in the gap, with decreasing shell thickness; both trends become more pronounced in the limit of the shell thickness tending to zero. Interestingly, there exists a wide dynamic range in $F_E(\lambda)$, from ∼7 to a maximum of ∼27 for gold but only from ∼24 to ∼37 in the case of silver, implying that a gold nanoshell has a greater impact on improving potential E-field enhancement than for silver. It should also be noted that the $F_E(\lambda)$ curves for gold are generally broader than for silver, for all shell thicknesses.

The COMSOL-generated $F_E(\lambda)$ curves are very slightly offset compared to the ME results, but the correlation between the two methods is qualitatively and quantitatively sound. With regards to the magnitude differences, both methods produce $F_E(\lambda)$ curves that are nicely superimposed on both sides of the resonance band where the error stabilizes around zero, for both silver and gold, and the greatest differences occur close to the resonance peaks. A possible explanation is that, as a result of the resonance phenomenon, the surface plasmons that are excited around the dimer's inner and outer surfaces in this wavelength range expose and amplify any differences between the two methods.

Effect of Dimer Separation, Δd. The effect of the dimer separation on the error between the two methods was investigated by fixing D and s and solving for $|E_z|$ as a function of separation distance d (Figure 3). The separations were decreased from $d = D = 20$ nm (100% of particle diameter), deemed as sufficiently far, down to $d = 1$ nm, which, even though possibly too small to realistically synthesize, was interesting from a meshing point of view. It should be noted that ∼4 mesh elements were fitted along the z-axis in the 1 nm gap to ensure an adequate spatial sampling of the interparticle space. This represents a spatial resolution of ∼0.25 nm and is the highest resolution necessary throughout this study.
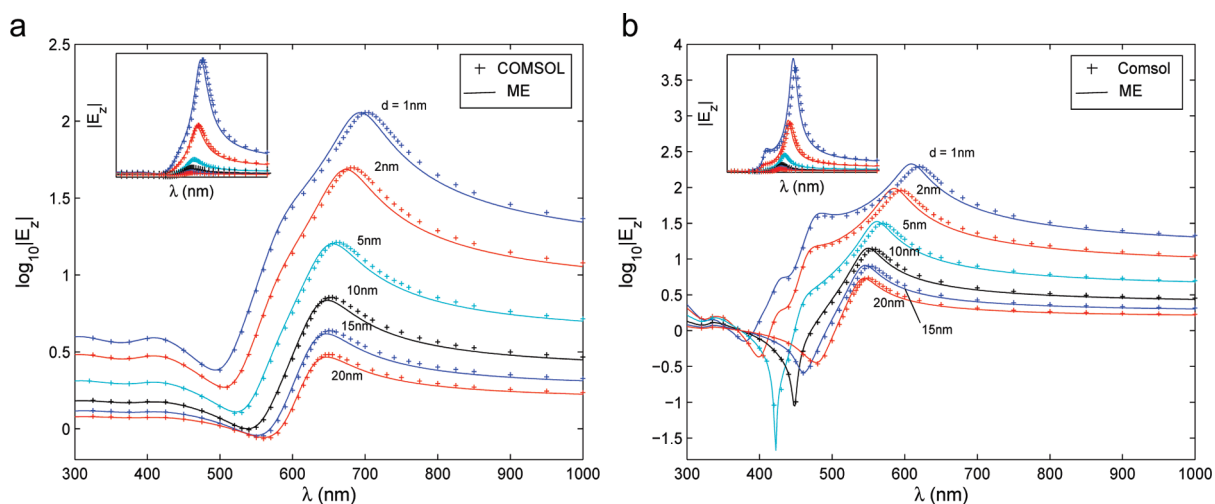
Figure 3. $F_E(\lambda)$ *vs* dimer separation d for ND [20 nm,Δd,20%] of (a) Au and (b) Ag.

As the dimer separation increases, the $F_E(\lambda)$ resonance bands of both gold and silver blue shift, tending toward the peak position of an isolated nanoshell as plasmon coupling between the dimers tends to zero. As a result of this reduced coupling with increasing separation, the $|E_z|$ magnitudes are also affected and dramatically decrease, requiring the $F_E(\lambda)$ curves to be plotted with a logarithmic y-axis for visualization purposes. The insets represent the original unscaled curves for reference. Once again, COMSOL generates $F_E(\lambda)$ curves that very closely resemble those of the ME, in that they superimpose about the resonance band, have closely correlated $|E_z|$ values, and are consistently red-shifted by a few nanometers.

Effect of Dimer Size, ΔD. The following test was performed to investigate the reliability of COMSOL to mesh the space and solve the electromagnetics problem in a narrow gap that is surrounded by two increasingly large objects. The dimers were increased from $D = 20$ to 150 nm, representing an experimentally relevant range of sizes, while keeping $d = 5$ nm and $s = 20\%$ (Figure 4).

The 3-D surface plots, generated by postprocessing in MatLab *via* a 2-D spline interpolation, highlight the progression of the $F_E(\lambda)$ resonance bands with increasing size. The divergence of the shape and position of $F_E(\lambda)$ between COMSOL and ME is obvious, with COMSOL producing a red shift over approximately a few hundred nanometers for both gold and silver in the former case, compared to about 50 nm for the two metals in the ME case. The rapidly increasing $F_E(\lambda)_{ME}$ diverges from $F_E(\lambda)_{COMSOL}$, which appears to plateau at ~50 for dimer sizes. The ME seems unable to properly solve for dimer nanoshells that start exceeding 20 nm, for which the quasi-static approximation appears to break down, due to the increasing influence of phase retardation effects.

A quantitative comparison between COMSOL and ME for each explored dimer scenario is concisely summarized in Figure 5, which focuses on the errors in three variables associated with the resonance band: relative error in $|E_z|$, $\Delta|E_z|$; shift of resonance λ_{max}, $\Delta\lambda_{peak}$; and relative error in fwhm, Δfwhm. These properties help
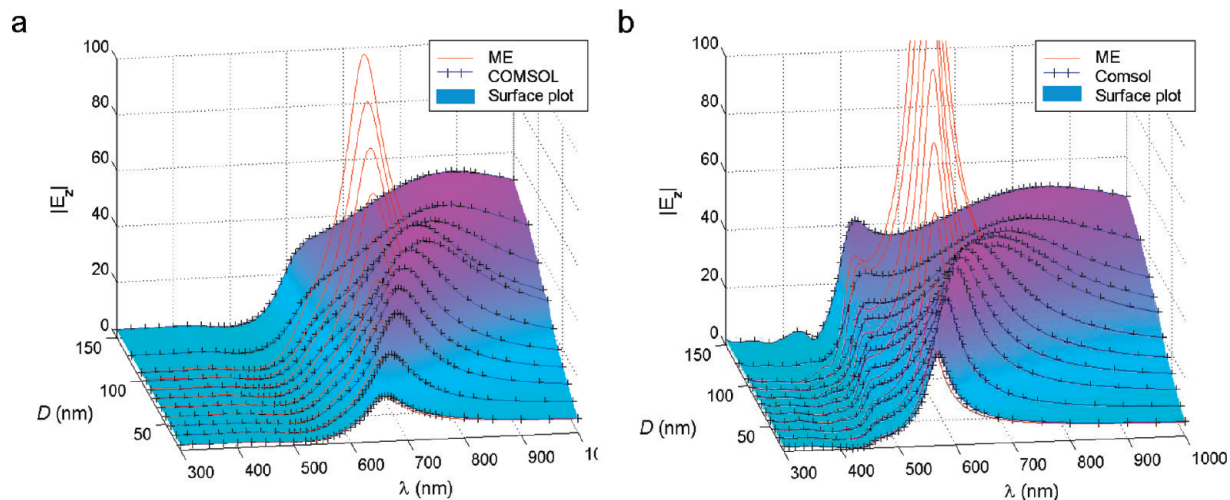

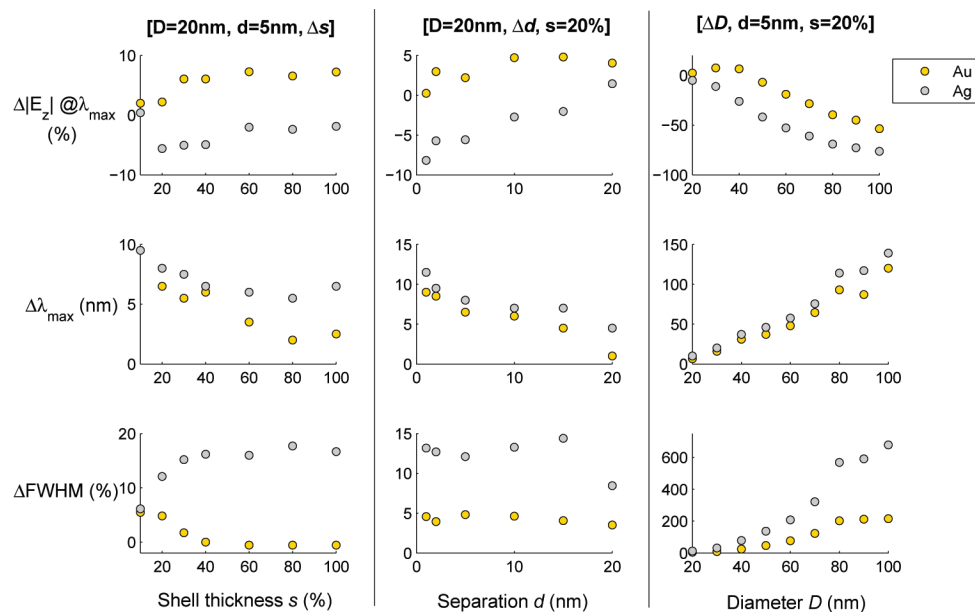Figure 4. $F_E(\lambda)$ *vs* nanoshell diameter D for ND [ΔD,5 nm,20%] of (a) Au and (b) Ag.

Figure 5. Matrix of error plots between COMSOL and ME for three scenarios of interest: ND [20 nm,5 nm,Δs], ND [20 nm,Δd,20%], and ND [ΔD,5 nm,20%]. Error computed as $\Delta \text{var} = \text{var}_{COMSOL} - \text{var}_{ME}$, where "var" represents the variable $|E_z|$, $\Delta \lambda_{max}$ or fwhm.

characterize the plasmon resonance band and are usually the features of greatest importance when developing and tuning nanostructures. The first, second, and third column convey scenarios ND [20 nm,5 nm,Δs], ND [20 nm,Δd,20%], and ND [ΔD,5 nm,20%], respectively. In each case, the errors were computed by evaluating $|E_z|_{COMSOL}$, fwhm$_{COMSOL}$, and $\lambda_{max-COMSOL}$ *relative* to $|E_z|_{ME}$, fwhm$_{ME}$, and λ_{max-ME}, respectively, that is

$$\Delta |E_z(\lambda)| = |E_z(\lambda)|_{COMSOL} - |E_z(\lambda)|_{ME}$$

As such, positive values indicate an overestimation by COMSOL and negative values suggest underestimation.

The shell thickness analysis is dealt with in the first column, which depicts a fairly stable, slightly increasing $\Delta |E_z|$ with increasing shell thickness, with $\Delta |E_z|$ averaging approximately 5% in the range (2%,6%) for gold and 4% in the range (0.5%,−6%) for silver. It is interesting to note that $|E_z|$ is overestimated for gold but underestimated for silver. The λ_{max} position is overestimated for both metals and decreases with increasing shell thickness in both cases, $\Delta \lambda_{peak}$ ranging (2%,7%) and (6%,9%) for gold and silver, respectively. The third graph of Δfwhm as a function of shell thickness conveys that gold starts with a ~6% error for the smallest shell thickness and decreases to stabilize around zero, implying that as the nanoshell core shrinks the plasmon bands become more similar. Interestingly, the opposite occurs for silver, with Δfwhm starting around ~7% and stabilizing close to 16%. It is crucial to remark, however, that this is a relative error, and considering the narrow widths of the thick-shelled silver dimers (Figure 2), such a high percentage, only maps to Δfwhm of only a few nanometers.

The second column of Figure 5 details this quantitative error analysis as a function of separation distance. Again, a fairly stable, slightly increasing $\Delta |E_z|$ with increasing separation is seen for gold, with an average ~4% in the range (0%,5%), whereas silver starts underestimated around −8% and increases to an overshoot of 2%. Both gold and silver follow a decreasing trend in $\Delta \lambda_{peak}$ with increasing separation, suggesting that accuracy improves as the particles become more isolated from each other. The last graph of the column conveys a stable, overestimated Δfwhm for both metals, averaging 5 and 12% for gold and silver, respectively. This last result suggests that the plasmon fwhm$_{COMSOL}$ is not critically affected by coupling between the two particles as the software is able to solve the geometries with a consistent offset from its analytical counterpart.

The third column of Figure 5 demonstrates the diverging behavior of the error variables between both methods, with increasing dimer size. In this case, however, the COMSOL results are used as the trusted baseline against which the ME is compared. In that regard, the ME increasingly overshoots $\Delta |E_z|$ for both metals (except for gold dimers $D < 50$ nm), and differences in λ_{max} and fwhm become more prominent as the dimers grow, really emphasizing the ME as suitably accurate for nanoshell dimer sizes $D \leq 20$ nm.

The discrepancy between an overestimated $|E_z|$ for gold but underestimated $|E_z|$ for silver, as observed across the first row of Figure 5, is intriguing since both silver and gold dimers were solved with identical meshing that yielded sufficiently converged solutions in both cases; further mesh refinement did not improve the obtained results. This effectively disqualifies meshing inconsistencies as the potential source of the ob-
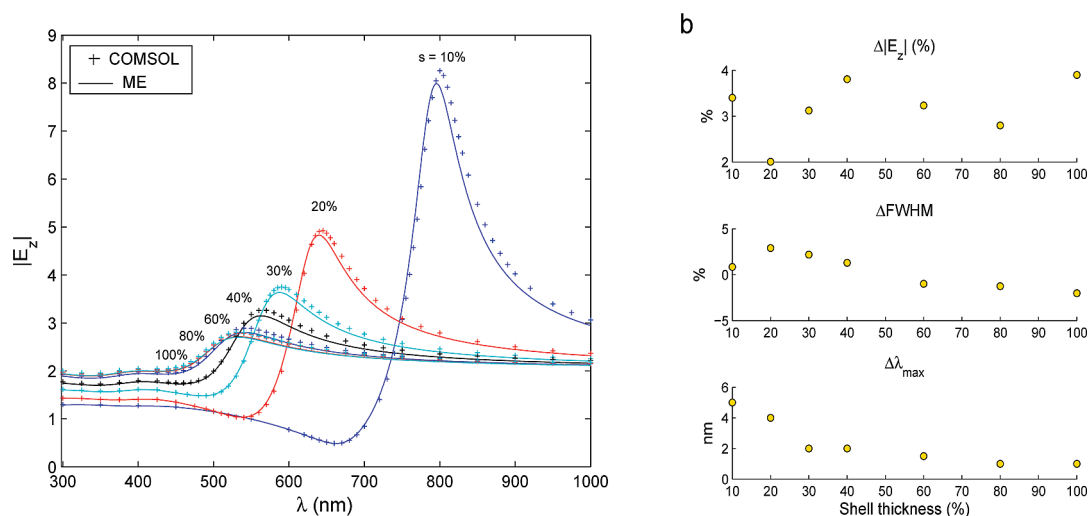
Figure 6. Analysis of 20 nm Au nanoshell monomer *vs* shell thickness *s*, interrogated at 2.5 nm from shell surface (a) $F_E(\lambda)$. (b) Relative error between ME and COMSOL.

served difference. Interestingly, the discrepancy appears to be consistent across dimer geometry, ND [*D*,*d*,*s*], and is therefore most probably material-specific in nature, arising from differences in the metal dielectric functions. The plasmon resonance peaks of gold and silver, at which $|E_z|$ is measured in each case, are effectively dictated by their corresponding dielectric function and occur at different wavelengths in the optical spectrum; this difference in resonance position could ostensibly affect the accuracy with which the fields in the vicinity of the dimer are solved by COMSOL's FEM algorithm. This would then result in over- or underestimation. Although further investigation into this phenomenon is beyond the scope of this paper, it is noteworthy that as long as the overshoot in either direction is consistent and small, as demonstrated here, COM-

SOL's FEM algorithm can still be trusted to generate reliable solutions.

The interesting λ_{peak} offsets of the $F_E(\lambda)$ curves seen in Figures 2, 3, and 4 between ME and COMSOL were further investigated by comparing the local E-field around a single nanoshell (monomer) to categorize it as a possible discrepancy introduced by the dimer configuration or an intrinsic difference related to the fundamental algorithms of each model. The E-field for the nanoshell monomer geometry was probed at a distance of 2.5 nm from the shell surface, effectively co-registering with the interrogation point in the dimer case. In the monomer case (Figure 6a), the two methods generated $F_E(\lambda)$ curves that are in good agreement with each other, yet an evident offset in resonance peak position and E-field magnitude is still present. The rela-
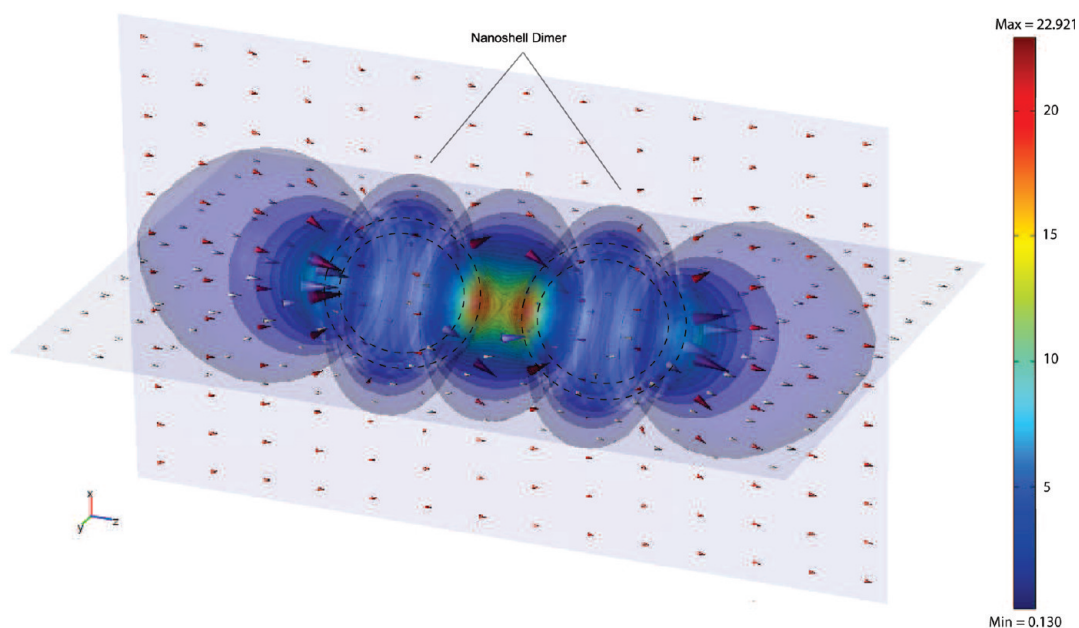

Figure 7. Three-dimensional illustration of E-field behavior surrounding gold dimer ND [20 nm,5 nm,20%] @ $\lambda_{peak} = 660$ nm.
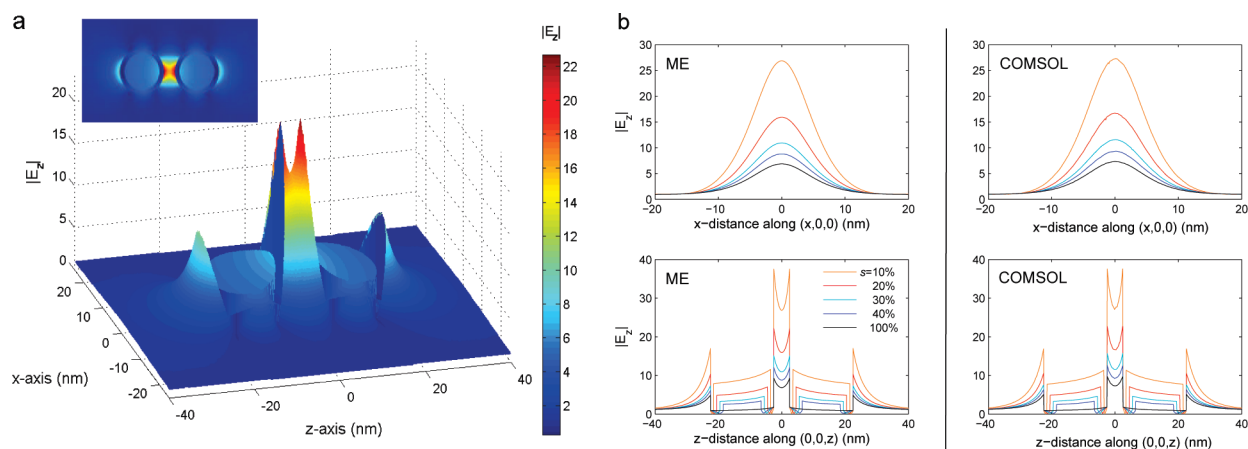
Figure 8. Spatial plots for Au ND [20 nm,5 nm,20%]: (a) slice plot along $x-z$ plane, represented in 3-D with $|E_z|$ as the third dimension. Inset is 2-D slice plot for reference. (b) Spatial resolution comparison of x- and z-line plots as a function of shell thickness s.

tive error between COMSOL and ME is presented in Figure 6b.

Very briefly, $\Delta|E_z|$ and Δfwhm do not display obvious trends, the former roaming around ~3% and the latter in the range ~(2%,3%). The shift in λ_{max}, however, decreases with increasing shell thickness and stabilizes around 1 nm in the limit $s \rightarrow r_2$. This analysis suggests that the observed $F_E(\lambda)$ offset potentially arises from algorithm-related, rather than dimer geometry-related, differences.

Analysis of the E-Field as a Function of Spatial Coordinate. For each selected wavelength, COMSOL solves the electromagnetic problem at every mesh node in 3-D space, which, although computationally intensive, enables 3-D spatial maps of the desired variable to be assembled and conveniently visualized. One such map for ND [20 nm,5 nm,20%] @ $\lambda_{peak} = 660$ nm is shown in Figure 7. The core and shell boundaries of the nanoshell dimer are delimited with dashed lines on either side of the separating junction. The 3-D surface contours represent isosurfaces of constant $|E_z|$, and the red and white arrows indicate the direction of the vector E_z on the $x-z$ and $y-z$ planes, respectively, and are proportional to the E-field strength at their position in 3-D space. This map depicts the concentrating and propagating behavior of the E-field in the vicinity of the dimers, as well as its rate of change away from the same. It is noteworthy that the arrows passing through the gap between the two nanoshells are purposefully withheld for better visual clarity; they would point from the left nanoshell to the right nanoshell.

For any method lacking a closed-form solution, spatial resolution is a critical measure and is dictated by the extent to which space is discretized into meshes for numerical solving. Figure 8a shows the $x-z$ slice of the 3D dimer system in Figure 7, with $|E_z|$ represented as the third dimension, and effectively conveys COMSOL's ability to smoothly mesh and solve the E-field around 3-D geometrical edges that bound domains of differing

dielectric functions. This plot also conveys that the maximum $|E_z|$ occurs at the metal/air interface, on either side of the gap, along the z-axis. The spatial resolution was investigated for ND [$D = 20$ nm,$s = 5$ nm] as a function of the shell thickness, evaluated at their corresponding plasmon peak wavelength (Figure 8b). The excellent agreement between the line profiles confirms that the 3-D meshing was dense enough, for all shell thicknesses, to effectively capture the features of interest, especially the abrupt E-field discontinuity at the dielectric boundaries. Unlike FDTD, which exhibits large errors at the nanoshell's interior or exterior boundaries,[19,20] FEM allows for a more versatile meshing algorithm that employs tetrahedrons to effectively discretize the shell's curved surface, such that the shell geometry is accurately maintained and solved for.

Computational Requirements. For completeness, it is appropriate to briefly discuss computational power and time differences between the two methods, as well as between COMSOL models solved in 2-D and 3-D space. This is illustrated in Table 1.

The results convey a huge range of times and powers that originates mostly from differences in the intrinsic problem-solving algorithms.

Several properties of the ME algorithm in this geometry resulted in exceptionally fast execution. In a calculation with many frequencies, the frequency-independent matrix elements computed only once. For each frequency, the linear system of equations is then solved for the ME coefficients, which takes little time since the system is relatively small. This system comprises $2N$ equations, where N is the number of multipole terms. In our calculations, we used $N = 20$ for all

TABLE 1. Computational Requirements for Generating a Single $F_E(\lambda)$ Curve

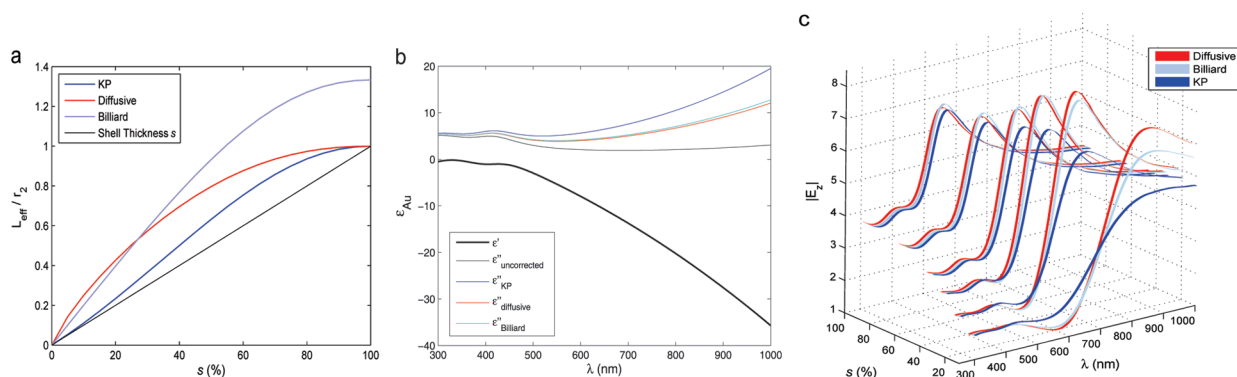|	ME	COMSOL 2-D	COMSOL 3-D
time	<1 min	5—10min	12—24h
RAM (Gb)	<1	~1	4—15

Figure 9. Comparison between the size correction models $L_{eff_{KP}}$, $L_{eff_{Diff}}$, and $L_{eff_{Bill}}$ for Au ND [20 nm, 5 nm, 20%]; (a) L_{eff} vs shell thickness s, (b) Au dielectric function, $\varepsilon_{Au}(\lambda)$, and (c) comparison of three L_{eff} models.

but the smallest dimer gaps; in the latter case, N was increased to 40. The relatively small number of terms in the multipole expansion is a direct result of the axial symmetry of the problem. Incrementing through 400 frequencies, the entire calculation in MatLab took typically less than a minute.

The generation of 3-D plots using COMSOL, however, is significantly more challenging. The extreme RAM loads for 3-D geometries in COMSOL are strongly dependent on the required meshing density for the particular geometry. The computational time, however, is affected not only by the meshing density but also more critically by the number of desired wavelength iterations; the sampling resolution of $F_E(\lambda)$ demonstrated in the above graphs (*i.e.*, 25−50 spectral points in the wavelength range of 300−1000 nm) requires 12−24 h. COMSOL meshes the geometry, obtaining the number of DoF required to solve for, and uses very large matrices in the 3-D case to solve the inverse problem for each electromagnetic quantity that appears in the original Maxwell's equations, whether or not they are desired by the user for the problem at hand. This is repeated for each wavelength of interest. As such, COMSOL effectively generates a 4-D volume of data for each electromagnetic variable ($\bar{\mathbf{E}}, \bar{\mathbf{H}}$, *etc.*), consisting of a field distribution in 3-D space with wavelength occupying the fourth dimension; although this routinely utilizes a couple of Gigabytes of hard drive storage, it is particularly convenient for probing electromagnetic quantities at any position in computational domain and at any solved wavelength, once the solution is achieved, allowing plots such as Figure 7 to be built and studied.

Given the long processing times and huge RAM utilized for 3-D geometries, there exists a memory limitation on the achievable meshing density (spatial sampling), as well as a compromise between spectral sampling and processing time, both which need consideration when solving complex geometries. Evidently, a numerical solver such as COMSOL would not be used for spherical geometries, where analytical methods such as the ME provide very accurate solutions for small

particles, but instead for an arbitrarily shaped geometry which the Mie scattering theory, and thus any Mie theory-derived approximation, are unable to accommodate.

Investigation of Small Size Effects. The aforementioned analysis used the Lorentz−Drude model for the dielectric function of both silver and gold and excluded any correction to account for a more experimentally valid analysis of the electromagnetic behavior of such small particles. Although several factors contribute toward tweaking the shape of the plasmon band,[41,42] the most prominent is the size effect, which results in its damping and broadening. The small size effect due to electron surface scattering at the particle boundaries becomes prominent as the metal thickness becomes smaller than the electron mean free path of a specific material. The electron mean free paths for gold and silver are approximately 50 nm,[43−45] and the size-limiting effect is encompassed in the "effective mean free path" variable, L_{eff}. Detailed comparison between experimental and calculated colloidal gold spectra has demonstrated that this size correction need only be applied to the imaginary part of the bulk metal dielectric function;[41,46] as such, L_{eff} only appears in ε'' (eq 5) and accounts for any additional loss incurred by the finite thickness of the nanoshell relative to the overall particle size. Here, λ_p is the wavelength of plasma oscillations, v_F and c are the Fermi velocity of electrons and the light velocity in vacuum, respectively. The dimensionless parameter A detailing the electron scattering process is taken as unity.[42,47]

Moroz[48] recently employed the nanoshell geometry to revisit a L_{eff} model, $L_{eff_{KP}}$ (eq 6), proposed by Kachan et al.,[49] and further proposed two models that are suggested to be more accurate: $L_{eff_{Diff}}$ (eq 7), derived by considering diffusive scattering, and $L_{eff_{Bill}}$ (eq 8), derived from the billiard scattering model. These three equations are plotted as a function of relative shell thickness in Figure 9. Note that eqs 6 and 7 differ only by the sign in the $(1 \pm q)$ term in front of the log normal function.

$$\varepsilon'' = \varepsilon''_{\text{bulk}} + \varepsilon''_{\text{correction}} = \varepsilon''_{\text{bulk}} + A\frac{\lambda_p}{L_{\text{eff}}}\frac{\nu_c}{2\pi c}\left(\frac{\lambda_0}{\lambda_p}\right)^3 \tag{5}$$

$$L_{\text{eff}_{KP}} = R\left[\frac{1}{1+q^2} - \frac{q}{2} - \frac{1}{4}\frac{1-q^2}{1+q^2}(1-q)\ln\frac{1-q}{1+q}\right] \tag{6}$$

$$L_{\text{eff}_{Diff}} = R\left[\frac{1}{1+q^2} - \frac{q}{2} - \frac{1}{4}\frac{1-q^2}{1+q^2}(1+q)\ln\frac{1-q}{1+q}\right] \tag{7}$$

$$L_{\text{eff}_{Bill}} = \frac{4}{3}R\frac{1-q^3}{1+q^2} \tag{8}$$

The variable L_{eff} is a real positive number that estimates the physical confinement experienced by electrons and is therefore inversely proportional to the constricting effects of the shell thickness. Its incorporation ultimately broadens the plasmon band and leads to a diminishing of the overall intensity of the local E-field in the vicinity of metal nanoparticles, effects that disappear only in the limit $L_{\text{eff}} \to \infty$ (eq 5). This implies that the size effect is to be accounted for regardless of the particle size, although the effects will rapidly fade away with increasing size as will be demonstrated shortly.

Figure 9a depicts the dependence of L_{eff}/r_2 on relative shell thickness, starting at the origin at increasing to 1 for $L_{\text{eff}_{KP}}$ and $L_{\text{eff}_{Diff}}$, but increasing beyond 1 for $L_{\text{eff}_{Bill}}$. This translates to corrections to the dielectric function of gold displayed in Figure 9b, which were evaluated for a shell thickness $s = 20\%$. The real part ε' is unaffected, but ε'' increases with decreasing L_{eff} for all λ. Figure 9c is a comparison between the $|E_z|$ spectra of the three models for ND [20 nm,5 nm,Δs] nanoshell dimers as a function of shell thickness. This plot clearly

emphasizes significant difference between them for thin shells, but they converge toward a similar E-field spectral profile in the limit $r_1 \to 0$.

In the remainder of the report, size effects are investigated using the $L_{\text{eff}_{KP}}$ model, first because it introduces the greatest loss of the three, enabling the study of the greatest impact size correction has on nanoparticle electromagnetics, and second due to the fact that it has already appeared as a size correction model in the literature.[50] Evidently, since all three boast similar behaviors, the trends depicted by $L_{\text{eff}_{KP}}$ will apply to the other two. The following section presents a quantitative comparison between uncorrected and size-corrected E-field spectra, using $L_{\text{eff}_{KP}}$, for both silver and gold as a function of shell thickness and size.

Figure 10a,b compares $F_E(\lambda)$ curves of ME (size-corrected) and COMSOL (uncorrected and size-corrected) for gold and silver, respectively. Thus far, it has been established that COMSOL is both qualitatively and quantitatively up to par with ME for small nanoparticles. The additional loss component in the dielectric function appears not to disrupt their correlation, as seen by their good agreement in both graphs.

The most striking feature is the significant $F_E(\lambda)$ damping and broadening experienced by the particles with thin shells for both gold and silver. For $s = 10\%$, gold experiences a $\sim$5-fold decrease in $|E_z|$ and a $\sim$65% fwhm broadening, whereas silver conveys a $\sim$6-fold decrease in $|E_z|$ and a $\sim$75% broadening. With increasing shell thickness, both damping and broadening diminish as L_{eff} reaches its maximum value for $s = r_2$.

The effect of the size correction on $F_E(\lambda)$ as a function of dimer size is presented in Figure 11, for which ND [ΔD,5 nm,20%] was employed. As observed throughout this analysis, the correction term affects the plasmon characteristics, rather than the off-resonance behavior of the particles. Indeed, in the
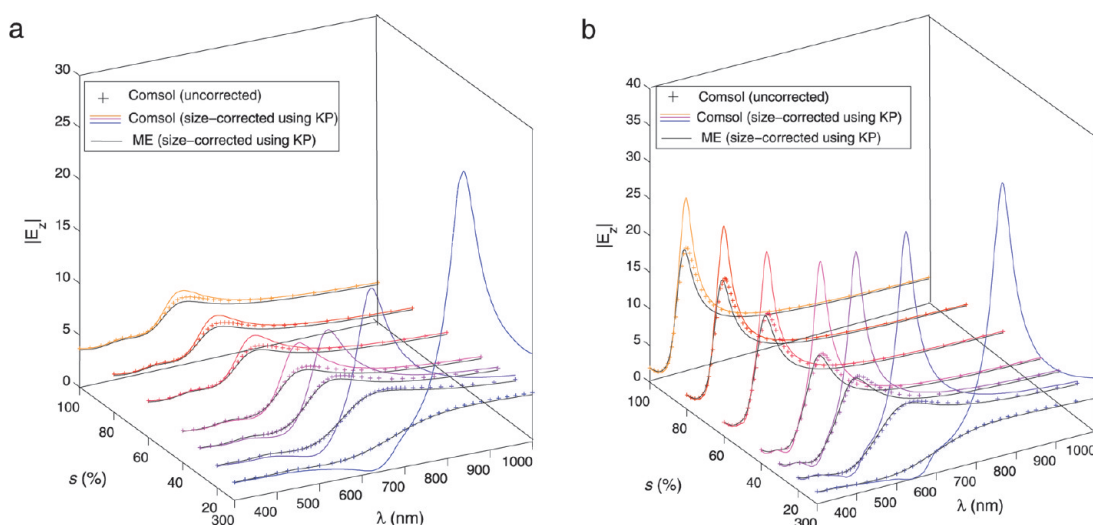

Figure 10. $F_E(\lambda)$ using $\varepsilon(\lambda)_{\text{uncorrected}}$ and $\varepsilon(\lambda)_{\text{corrected}}$ as a function of shell thickness s for ND [20 nm,5 nm,Δs] of (a) Au and (b) Ag.
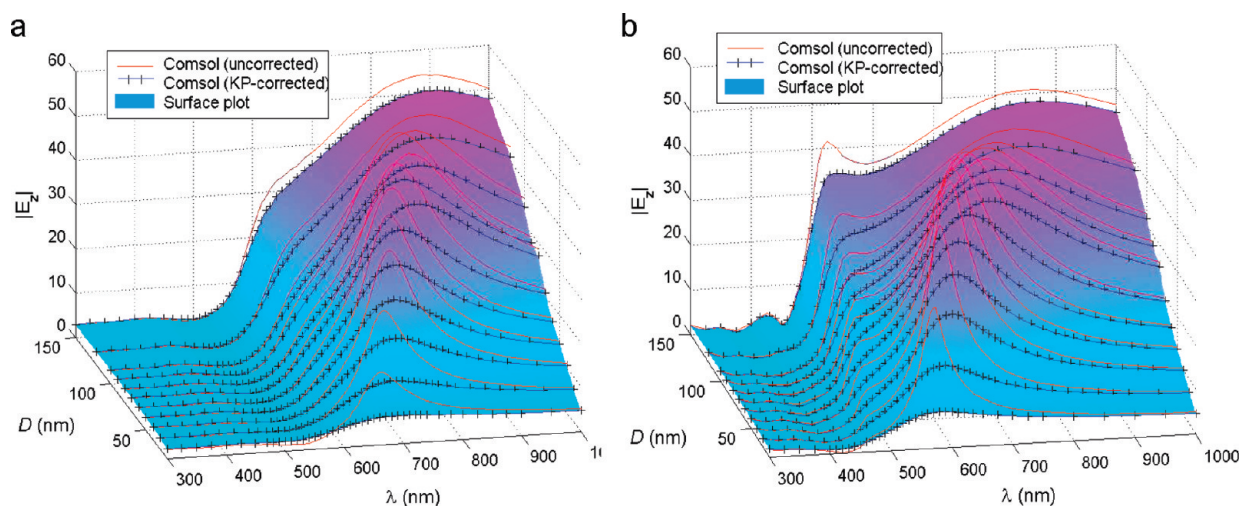
Figure 11. $F_E(\lambda)$ using $\varepsilon(\lambda)_{corrected}$ *vs* nanoshell diameter D, for ND [ΔD,5 nm,20%] of (a) Au and (b) Ag.

range of 300−500 nm for gold and 300−400 nm for silver, the uncorrected and corrected versions as functions of shell thickness and dimer size are practically identical. They also converge in the long-wavelength limit. In addition, it is noteworthy that there still exists substantial error for the 150 nm nanoshells, which suggests that the correction term cannot be ignored even at these sizes and relative shell thicknesses.

Finally, these results are summarized in Figure 12. The first column unanimously shows that the difference between uncorrected and size-corrected $F_E(\lambda)$ tends toward zero as shell thickness increases. In addition to significant damping and broadening for thin shells, a substantial red shift of the size-corrected curves also takes place, which is more pronounced for gold (λ_{max} = 50 nm) than for silver (λ_{max} = 27 nm). The $\Delta|E_z|$ and Δfwhm variables show greater deviation for silver than for gold; however, the error seems to plateau for thicknesses greater than 40% in all three cases.

The second column reiterates the trends observed with the data in Figure 10, with resonance damping, broadening, and red shifting all being greatest for small particles and reducing with increasing particle size. Interestingly, both metals appear to be more consistent with each other.

As a final note, it is of experimental interest to mention the impact of variations in the nanoshell dimer geometry on the SERS enhancement factor, $SERS_{EF}$, which is aforementioned to be approximately proportional to $|E_z|^4$. The maximum SERS enhancement factors achieved in the dimer gap using $\varepsilon(\lambda)_{uncorrected}$ are extracted from Figures 2, 3, and 4. The thinnest shell of 10% yielded $SERS_{EF} \sim 27^4 = 5.3E5$ and $\sim 37^4 = 1.9E6$ for Au and Ag, respectively. The smallest interparticle distance of 1 nm produced $SERS_{EF} \sim 118^4 = 1.9E8$ and $\sim 200^4 = 1.6E9$ for Au and Ag, respectively. With respect to dimer size, the 90 and 50 nm dimers were the strongest for Au and Ag, respectively, both interestingly generate $SERS_{EF} \sim 56^4 = 9.8E6$. These are very large $SERS_{EF}$ and would suggest that synthesizing extremely thin-shelled dimers that are very close to each other would yield even stronger enhancements. This is not the case, unfortunately, since the $SERS_{EF}$ are dramatically reduced with the incorporation of the size effect, reflected in Figure 10 and Figure 11. For
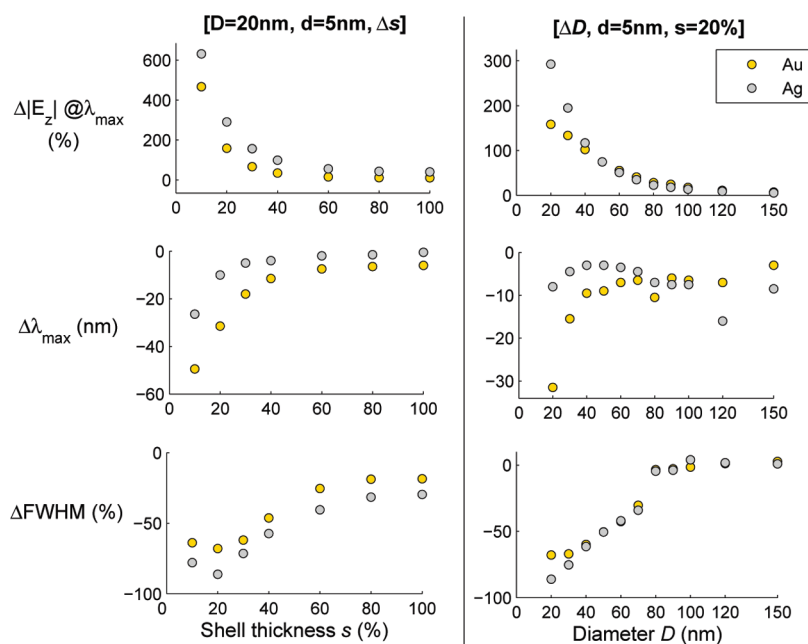

Figure 12. Error between models employing $\varepsilon(\lambda)_{uncorrected}$ and $\varepsilon(\lambda)_{corrected}$. The error is evaluated as follows: Δvar = var$_{COMSOL-uncorrected}$ − var$_{COMSOL-corrected}$, where "var" represents the variable $|E_z|$, $\Delta\lambda_{max}$, or fwhm.

the same shell thickness, the SERS$_{EF}$ of both Au and Ag are reduced to a mere $\sim 5^4 = 625$! The dramatic changes brought about by the fourth power factor, used to estimate the SERS enhancement, emphasize the importance of considering the size effect to yield accurate models, especially for the design and characterization of small particles for use in SERS applications.

The COMSOL Multiphysics numerical simulation package is a versatile tool that can be confidently used for nanoscale electromagnetics of 3-D geometries. Although it is memory-intensive, the obtained result is accurate, as a function of both wavelength and space, to within a few percent of its theoretical counterpart; it additionally provides the ability to truly investigate the plasmonic behavior within and without a nanostructure of interest, which can then be reconciled with experimental analysis. In order to achieve this, however, it is important to emphasize that the size dependence is of crucial importance, especially when dealing with the nanoshell geometry, for which electron mean free path models have been derived. COMSOL's agile meshing algorithm and resulting solution accuracy would suggest it to be a more promising computational electrodynamics modeling tool than FDTD-based packages for use in the plasmonics arena.

METHODS

The numerical simulations were performed with the commercial software package COMSOL Multiphysics (version 3.4 with incorporated RF module, installed on a dual-Quad Core 32GB RAM workstation), which comprises electromagnetic code based on the finite element method (FEM) (http://www.comsol.com).

The computational domain containing the nanoparticle system of interest was delimited by perfectly matched layers (PMLs) that efficiently absorb any scattering off the particles, thereby preventing any unwanted reflections in the domain. Adequate meshing of the geometry of interest is a critical step in a FEM simulation since the spatial resolution in the computational domain needs to be high enough to capture fast changing geometries, which directly translates to solution accuracy. A new spatial mesh was interactively constructed for each unique variable combination ND [D,d,s] to ensure that the E-field was properly solved at the position (0,0,0). The meshing was considered sufficiently dense when little variation in the second decimal place of the solved $|E_z|$ was observed. In 3-D space, meshes usually consisted of between 180k and 350k points, representing between 1 and 2.7 M DoF. This number decreased significantly in 2-D to between 10k and 20k, corresponding to tens of thousands of DoF.

The spectral domain was sampled finely enough to ensure any rapid change in the spectrum would be captured with sufficient resolution to accurately compare both computational methods. This was especially critical around the plasmon resonance peak in all cases, and finer sampling was also required in regions where the trend was uncertain, such as the 400−500 nm wavelength range for the silver dimers. The ME produced $F_E(\lambda)$ sampled at 2.5 nm wavelength intervals, whereas the spectral resolution in COMSOL was dynamically selected according to the important features observed in $F_E(\lambda)$, thus varying between 5 and 50 nm wavelength intervals.

The presented data were assembled using MatLab and COMSOL's in-house postprocessing environment.

REFERENCES AND NOTES

1. Kneipp, K.; Kneipp, H.; Manoharan, R.; Hanlon, E. B.; Itzkan, I.; Dasari, R. R.; Feld, M. S. Extremely Large Enhancement Factors in Surface-Enhanced Raman Scattering for Molecules on Colloidal Gold Clusters. *Appl. Spectrosc.* **1998**, *52*, 1493–1497.
2. Kneipp, K.; Kneipp, H.; Itzkan, I.; Dasari, R. R.; Feld, M. S. Surface-Enhanced Raman Scattering and Biophysics. *J. Phys.: Condens. Matter* **2002**, *14*, 597–624.
3. Nie, S.; Emory, S. R. Probing Single Molecules and Single Nanoparticles by Surface-Enhanced Raman Scattering. *Science* **1997**, *275*, 1102–1106.
4. Vo-Dinh, T.; Hiromoto, M.; Begun, G. M.; Moody, R. L. Surface-Enhanced Raman Spectroscopy for Trace Organic Analysis. *Anal. Chem.* **1984**, *56*, 1667.
5. Vo-Dinh, T.; Houck, K.; Stokes, D. L. Surface-Enhanced Raman Gene Probes. *Anal. Chem.* **1995**, *66*, 3379.
6. Vo-Dinh, T. Surface-Enhanced Raman Spectroscopy Using Metallic Nanostructures. *Trends Anal. Chem.* **1998**, *17*, 557.
7. Vo-Dinh, T.; Stokes, D. L. Surface-Enhanced Raman Detection of Chemical Vapors and Aerosols Using Personal Dosimeters. *Field Anal. Chem. Technol.* **1999**, *3*, 346.
8. Vo-Dinh, T.; Allain, L. R.; Stokes, D. L. Cancer Gene Detection Using Surface-Enhanced Raman Scattering (SERS). *J. Raman Spectrosc.* **2002**, *33*, 511.
9. Wabuyele, M.; Vo-Dinh, T. Detection of HIV Type 1 DNA Sequence Using Plasmonics Nanoprobes. *Anal. Chem.* **2005**, *77*, 7810–7815.
10. Khoury, C. G.; Vo-Dinh, T. Gold Nanostars For Surface-Enhanced Raman Scattering: Synthesis, Characterization and Optimization. *J. Phys. Chem. C* **2008**, *112*, 18849–18859.
11. Wang, H.-N.; Vo-Dinh, T. Multiplex Detection of Breast Cancer Biomarkers Using Plasmonic Molecular Sentinel Nanoprobes. *Nanotechnology* **2009**, *20*, 065101–065107.
12. Tang, X.-L.; Jiang, P.; Ge, G.-L.; Tsuji, M.; Xie, S.-S.; Guo, Y.-J. Poly(*N*-vinyl-2-pyrrolidone) (PVP)-Capped Dendritic Gold Nanoparticles by a One-Step Hydrothermal Route and Their High SERS Effect. *Langmuir* **2008**, *24*, 1763–1768.
13. Orendorff, C. J.; Gearheart, L.; Jana, N. R.; Murphy, C. J. Aspect Ratio Dependence on Surface Enhanced Raman Scattering Using Silver and Gold Nanorod Substrates. *Phys. Chem. Chem. Phys.* **2006**, *8*, 165–170.
14. McLellan, J. M.; Siekkinen, A.; Chen, J.; Xia, Y. Comparison of the Surface-Enhanced Raman Scattering on Sharp and Truncated Silver Nanocubes. *Chem. Phys. Lett.* **2006**, *427*, 122–126.
15. Driskell, J. D.; Lipert, R. J.; Porter, M. D. Labeled Gold Nanoparticles Immobilized at Smooth Metallic Substrates: Systematic Investigation of Surface Plasmon Resonance and Surface-Enhanced Raman Scattering. *J. Phys. Chem. B* **2006**, *110*, 17444–17451.
16. Hicks, E. M.; Lyandres, O.; Hall, W. P.; Zou, S.; Glucksberg, M. R.; Duyne, R. P. V. Plasmonic Properties of Anchored Nanoparticles Fabricated by Reactive Ion Etching and Nanosphere Lithography. *J. Phys. Chem. C* **2007**, *111*, 4116–4124.
17. Min, Q.; Santos, M. J. L.; Girotto, E. M.; Brolo, A. G.; Gordon, R. Localized Raman Enhancement from a Double-Hole Nanostructure in a Metal Film. *J. Phys. Chem. C* **2008**, *112*, 15098–15101.
18. Grand, J.; Kostcheev, S.; Bijeon, J.-L.; de la Chapelle, M. L.; Adam, P.-M.; Rumyantseva, A.; Lerondel, G.; Royer, P. Optimization of SERS-Active Substrates for Near-Field Raman Spectroscopy. *Synth. Met.* **2003**, *139*, 621–624.

19. Oubre, C.; Nordlander, P. Finite Difference Time Domain Studies of Optical Properties of Nanoshell Structures. *Proc. SPIE* **2003**, *5221*, 133–143.

20. Dhawan, A.; Norton, S. J.; Gerhold, M. D.; Vo-Dinh, T. Comparison of FDTD Numerical Computations and Analytical Multipole Expansion Method for Plasmonics-Active Nanosphere Dimers. *Opt. Express* **2009**, *17*, 9688–9703.

21. Oubre, C.; Nordlander, P. Finite-Difference Time-Domain Studies of the Optical Properties of Nanoshell Dimers. *J. Phys. Chem. B* **2005**, *109*, 10042–10051.

22. Chau, Y.-F.; Yeh, H.-H.; Tsai, D. P. Near-Field Optical Properties and Surface Plasmon Effects Generated by a Dielectric Hole in a Silver-Shell Nanocylinder Pair. *Appl. Opt.* **2008**, *47*, 5557–5567.

23. Cui, X.; Erni, D. Enhanced Propagation in a Plasmonic Chain Waveguide with Nanoshell Structures Based on Low- And High-Order Mode Coupling. *J. Opt. Soc. Am. A* **2008**, *25*, 1783–1789.

24. Chau, Y.-F.; Yeh, H. H.; Tsai, D. P. Surface Plasmon Effects Excitation from Three-Pair Arrays of Silver-Shell Nanocylinders. *Phys. Plasmas* **2009**, *16*, 022303.

25. Issa, N. A.; Guckenberger, R. Optical Nanofocusing on Tapered Metallic Waveguides. *Plasmonics* **2007**, *2*, 31–37.

26. Brown, R. J. C.; Wang, J.; Milton, M. J. T. Electromagnetic Modelling of Raman Enhancement from Nanoscale Structures as a Means to Predict the Efficacy of SERS Substrates. *J. Nanomater.* **2007**, *2007*, 12086–12096.

27. Knorr, I.; Christou, K.; Meinertz, J.; Selle, A.; Ihlemann, J.; Marowsky, G. Prediction and Optimization of Surface-Enhanced Raman Scattering Geometries Using COMSOL Multiphysics. *Proc. COMSOL Conf. Hannover*, 2008.

28. Ehrhold, K.; Christiansen, S.; Gosele, U. Plasmonic Properties of Bimetal Nanoshell Cylinders and Spheres. *Proc. COMSOL Conf. Hannover*, 2008.

29. Gerardy, J. M.; Ausloos, M. Absoprtion Spectrum of Clusters of Spheres from the General Solution of Maxwell'S Equations. The Long-Wavelength Limit. *Phys. Rev. B* **1980**, *22*, 4950–4959.

30. Norton, S. J.; Vo-Dinh, T. Optical Response of Linear Chains of Metal Nanopsheres and Nanospheroids. *J. Opt. Soc. Am.* **2008**, *25*, 2767–2775.

31. Brandl, D. W.; Oubre, C.; Nordlander, P. Plasmon Hybridization in Nanoshell Dimers. *J. Chem. Phys.* **2005**, *123*, 024701-1–024701-11.

32. Lassiter, J. B.; Aizpurua, J.; Hernandez, L. I.; Brandl, D. W.; Romero, I.; Lal, S.; Hafner, J. H.; Nordlander, P.; Halas, N. J. Close Encounters between Two Nanoshells. *Nano Lett.* **2008**, *8*, 1212–1218.

33. Averitt, R. D.; Sarkar, D.; Halas, N. J. Plasmon Resonance Shifts of Au-Coated Au2s Nanoshells: Insight into Multicomponent Nanoparticle Growth. *Phys. Rev. Lett.* **1997**, *78*, 4217–4220.

34. Ru, E. C. L.; Etchegoin, P. G. Rigorous Justification of the $|E|^4$ Enhancement Factor in Surface Enhanced Raman Spectroscopy. *Chem. Phys. Lett.* **2006**, *423*, 63–66.

35. Palik, E. D. *Handbook of Optical Constants of Solids*; Academic Press: San Diego, CA, 1998.

36. Liz-Marzan, L. M.; Giersig, M.; Mulvaney, P. Synthesis of Nanosized Gold−Silica Core−Shell Particles. *Langmuir* **1996**, *12*, 4329–4335.

37. Bergna, H. E.; Roberts, W. O. *Colloidal Silica: Fundamentals and Applications*; CRC Press: Boca Raton, FL, 2006.

38. Kerker, M. Electromagnetic Model for Surface-Enhanced Raman Scattering (SERS) on Metal Colloids. *Acc. Chem. Res.* **1984**, *17*, 271–277.

39. Mishchenko, M. I.; Hovenier, J. W.; Travis, L. D. *Light Scattering by Nonspherical Particles*; Academic Press: New York, 2000.

40. Kerker, M. *Scattering of Light and Other Electromagnetic Radiation*; Academic Press: New York, 1969.

41. Khlebtsov, N. G.; Bogatyrev, V. A.; Dykman, L. A.; Melnikov, A. G. Spectral Extinction of Colloidal Gold and Its Biospecific Conjugates. *J. Colloid Interface Sci.* **1996**, *180*, 436–445.

42. Westcott, S. L.; Jackson, J. B.; Radloff, C.; Halas, N. J. Relative Contributions to the Plasmon Line Shape of Metal Nanoshells. *Phys. Rev. B* **2002**, *66*, 155431(1−5).

43. Ashcroft, N. W.; Mermin, N. D. *Solid State Physics*; Saunders College: Philadelphia, 1976.

44. Kittel, C. *Introduction to Solid State Physics*; Wiley: New York, 1996.

45. Kreibig, U.; Fragstein, C. V. The Limitation of Electron Mean Free Path in Small Silver Particles. *Z. Phys.* **1969**, *224*, 307–323.

46. Scaffardi, L. N.; Pellegri, N.; de Sacntis, O.; Tocho, J. O. Sizing Gold Nanoparticles by Optical Extinction Spectroscopy. *Nanotechnology* **2005**, *16*, 158–163.

47. Coronado, E. A.; Schatz, G. C. Surface Plasmon Broadening for Arbitrary Shape Nanoparticles: A Geometrical Probability Approach. *J. Chem. Phys.* **2003**, *119*, 3926–3934.

48. Moroz, A. Electron Mean Free Path in a Spherical Shell Geometry. *J. Phys. Chem. C* **2008**, *112*, 10641–10652.

49. Kachan, S. M.; Ponyavina, A. N. Resonance Absorption Spectra of Composites Containing Metal-Coated Nanoparticles. *Mol. Struct.* **2001**, *267*, 563–564.

50. Khlebtsov, B.; Khlebtsov, N. Ultrasharp Light-Scattering Resonances of Structured Nanospheres: Effects of Size-Dependent Dielectric Functions. *J. Biomed. Opt.* **2006**, *11*, 044002(1−5).